ICANS-XIV
14th Meeting of the International Collaboration on
Advance Neutron Sources
June 14–19, 1998
Utica, IL USA

CRYOGENIC MODERATOR SIMULATIONS: CONFRONTING REALITY

E. B. Iverson, J. M. Carpenter
Intense Pulsed Neutron Source
Argonne National Laboratory
9700 South Cass Avenue
Argonne, IL USA 60439

The Intense Pulsed Neutron Source (IPNS) at Argonne National Laboratory is a spallation neutron source dedicated to materials research. Its three cryogenic methane moderators provide twelve neutron beams to fourteen instruments and test facilities. This report concerns ongoing activities for benchmarking our Monte Carlo model of the IPNS neutron generation system.[1] This paper concentrates on the techniques (both experimental and calculational) used in such benchmarking activities.

1 IPNS Description

IPNS is a spallation neutron source in which protons are accelerated to 450 MeV and directed into a light water-cooled target composed of depleted uranium disks. A rough schematic of the target, reflector, and moderator system appears in Figure 1. The IPNS accelerator system delivers some 15 μA (time-averaged) of protons in bursts less than 100 ns long at a rate of 30 Hz. The horizontal uranium target, 250 mm long and 100 mm in diameter, is surrounded by a (vertical) graphite inner reflector 250 mm in diameter, and a beryllium outer reflector 600 mm in diameter. There are three cryogenic moderators, each decoupled from the reflector by 0.5 mm of cadmium. The "F" moderator is below the front of the uranium target (the end near the proton beam), and is composed of liquid methane (CH_4) at 100 K. The "F" moderator is 100 by 100 by 45 mm in size, and is poisoned with gadolinium 16 mm below the large faces, both of which are viewed by beam ports. The "H" moderator is above the front of the uranium target, and consists of solid methane at 30 K. The "H" moderator is also 100 by 100 by 45 mm in size, and is poisoned with gadolinium at the centerline. For both the "F" and "H" moderators, the poisoning is provided by 0.5 mm thick sheets of a gadolinium-aluminum alloy containing 17.2 weight percent gadolinium. The "C" moderator is below the rear of the uranium target, and is also solid methane at 30 K. The "C" moderator is an un-poisoned, re-entrant moderator, 100 by 100 by 80 mm, with horizontal grooves 40 mm deep and 10 mm high in the viewed face.

2 Compared Quantities

The quantities examined in benchmarking our system include the neutron energy-dependent intensity of the neutron beams and the neutron energy-dependent emission time distributions of the neutron beams. While these do not provide a complete description of the moderator's performance, such as might be required for the optimized design of a scattering instrument, these two quantities do encompass the most significant characteristics of a neutron beam.

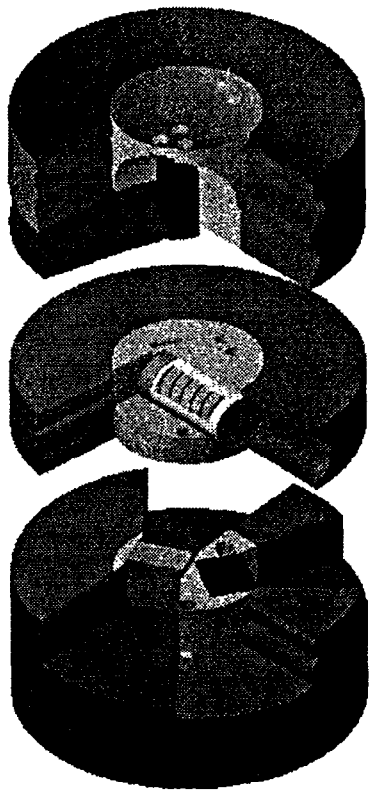

Figure 1: The IPNS target, reflector, and moderator system. Protons enter from the rear on the left in this view.

2.1 Intensity

The neutron beam intensity emitted from the moderator faces, normalized by the accelerator beam current, corresponds to what in optics terminology is a normalized "luminous intensity." This intensity is related to a measured flux;

$$i(E) = \frac{L^2}{I}\,\phi(E)|_L\,, \tag{1}$$

where $\phi(E)$ is the time-averaged flux per unit energy at a distance L far from the moderator face, and I is the time-averaged accelerator beam current. In general, the use of the luminous intensity rather than flux as a metric permits the brightness of the moderator face to be specified independently from the length of the flight path. For this metric to be useful for a re-entrant moderator such as the IPNS "C" moderator, the distance L must be either large enough that there is no significant self-shielding of the moderator face, or L must be similar to the actual distance from the real moderator to the real sample. The units of $i(E)$ are then neutrons per steradian per second per electron-Volt per micro-ampere. The commonly-quoted measure of moderator coupling effectiveness is then

$$[E \times i(E)]|_{E=1\text{ eV}}\,. \tag{2}$$

If the intensity $i(E)$ is multiplied by E, the resulting quantity is proportional to the normalized counting rate seen in a thin $1/v$ detector placed at a distance L from the moderator surface, scaled by a factor which is independent of neutron energy. Thus $E \times i(E)$ is easily compared to a time-of-flight beam intensity measurement. This quantity is calculated directly in the Monte Carlo simulations, using point detectors as

described below.

A combination of gold foil activation and time-of-flight spectrum measurements provides the absolutely normalized true intensities for the various neutron beams.[2] A low efficiency $1/v$-detector operated in a counting mode records the intensity of the neutron beam, while a cadmium-difference gold foil activation measurement (performed at the same time) provides the scale factor for the detector efficiency, and thus the absolutely normalized detector output.

The time-averaged counting rate per unit time-of-flight at time-of-flight t at the beam monitor is

$$C(t) = A\eta(E)\phi_{\mathrm{D}}(E)\frac{2E}{t} + B, \tag{3}$$

where E is the neutron energy corresponding to time-of-flight t, A is the area of the beam intercepted by the detector, η is the energy-dependent efficiency of the detector at energy E, ϕ_{D} is time-averaged flux per unit energy at the detector, and B is a steady background counting rate. For thin $1/v$-detectors (r.g., ^{3}He in ^{4}He or BF_3 in P-10), the efficiency can be expressed as

$$\eta(\lambda) = k\lambda, \tag{4}$$

where λ is the neutron wavelength corresponding to energy E, and k is a constant unique to each detector and electronic setup. Substituting Equation 4 into Equation 3, together with the de Broglie relation, gives

$$C(t) = E \times \phi_{\mathrm{D}}(E)\frac{2hkA}{mL_D} + B, \tag{5}$$

where h is Planck's constant, m is the mass of the neutron, and L_D is the length of the flight path between the moderator and the detector. We can then define an absolute efficiency (that accounts for detector geometry and position as well as intrinsic efficiency)

$$K' = \frac{2hkA}{mL_D}, \tag{6}$$

relating the flux at the detector position to the counting rate such that

$$\phi_{\mathrm{D}}(E) = \frac{C(t) - B}{EK'}. \tag{7}$$

We can modify Equation 7 to relate the flux at the foil position to the net counting rate at the detector position,

$$\phi_{\mathrm{f}}(E) = \frac{C(t) - B}{EK} = \frac{\tilde{C}(t)}{EK}, \tag{8}$$

where K is a scaled absolute efficiency

$$K = K'\frac{L_{\mathrm{f}}^2}{L_{\mathrm{D}}^2}. \tag{9}$$

Equation 8 is especially useful, as the time-averaged counting rate per unit time-of-flight $C(t)$ is easily obtained from the beam monitor, the background B is a constant at all time-of-flight values t, and the efficiency K will remain the same for any given detector, providing that the detector's configuration (e.g., discriminator setting, etc.) is not changed. In contrast, the intrinsic efficiency k is nominally provided by the manufacturer, as calculated from the cross section of the detecting medium, and its use requires knowledge of many other parameters.

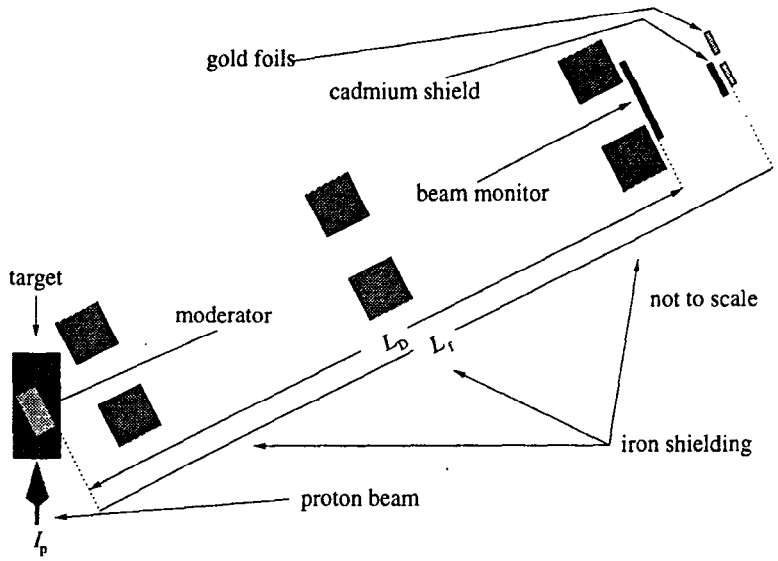

Figure 2: Experimental layout for cadmium-difference gold foil activation measurements.

To measure the efficiency K of a particular detector in a given configuration, consider a cadmium-difference gold foil activation measurement, performed downstream from this beam monitor, as in Figure 2. The neutron activation rate in the bare foil R_b is

$$R_b = N_b \int_0^\infty \sigma_{Au} \phi \, dE, \tag{10}$$

where N_b is the total number of atoms of gold in the foil and σ_{Au} is the microscopic activation cross section. For the covered foil,

$$R_c = N_c \int_0^\infty e^{-\Sigma_{Cd} s} \sigma_{Au} \phi \, dE, \tag{11}$$

where R_c and N_c apply to the covered foil, and Σ_{Cd} and s are the macroscopic total cross section and the physical thickness, respectively, for the cadmium cover. Rearranging Equations 10 and 11 and taking their difference gives

$$\frac{R_b}{N_b} - \frac{R_c}{N_c} = \int_0^\infty (1 - e^{-\Sigma_{Cd} s}) \sigma_{Au} \phi \, dE. \tag{12}$$

The quantity $(1 - e^{-\Sigma_{Cd} s})$ is very small and approximately constant at energies greater than the cadmium cutoff. If we define γ as a constant equal to the mean transmission through the cadmium cover for all energies above some energy E_1, and divide our range of integration at E_1, we have

$$\frac{R_b}{N_b} - \frac{R_c}{N_c} = \int_0^{E_1} (1 - e^{-\Sigma_{Cd} s}) \sigma_{Au} \phi \, dE + \gamma \int_{E_1}^\infty \sigma_{Au} \phi \, dE. \tag{13}$$

The second integrand in Equation 13 is from Equation 10—only the limits are different. We can therefore say

$$\begin{aligned} \frac{R_b}{N_b} - \frac{R_c}{N_c} &= \int_0^{E_1} (1 - e^{-\Sigma_{Cd} s}) \sigma_{Au} \phi \, dE - \gamma \int_0^{E_1} \sigma_{Au} \phi \, dE + \gamma \int_0^\infty \sigma_{Au} \phi \, dE \\ &= \int_0^{E_1} (1 - e^{-\Sigma_{Cd} s} - \gamma) \sigma_{Au} \phi \, dE + \gamma \frac{R_b}{N_b}. \end{aligned} \tag{14}$$

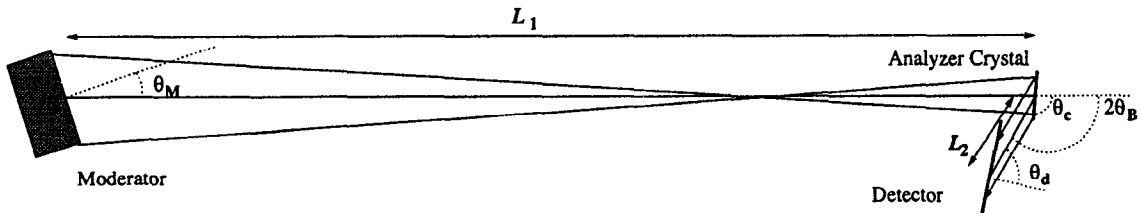

Figure 3: Experimental layout for time-focused pulse shape measurements.

Combining Equation 8 with Equation 14 and converting the integral in Equation 14 from energy to time-of-flight, then

$$\frac{R_b}{N_b}(1-\gamma) - \frac{R_c}{N_c} = \frac{2}{K}\int_{t_1}^{\infty}(1 - e^{-\Sigma_{Cd}s} - \gamma)\sigma_{Au}\frac{\tilde{C}(t)}{t}\,dt, \tag{15}$$

where the cross sections are now expressed as a function of time-of-flight, and t_1 is the time-of-flight for neutrons of energy E_1.

At very long times t, the counting rate $C(t)$ approaches B, thus allowing the upper limit of the integral in Equation 14 to be changed from ∞ to some t_2. We can now solve Equation 15 for K,

$$K = \frac{2N_cN_b}{N_cR_b(1-\gamma) - N_bR_c}\int_{t_1}^{t_2}(1 - e^{-\Sigma_{Cd}s} - \gamma)\sigma_{Au}\frac{\tilde{C}(t)}{t}\,dt. \tag{16}$$

The flux as a function of energy at the sample position can then be calculated as

$$\phi(E) = \frac{\tilde{C}(t)\,(N_cR_b(1-\gamma) - N_bR_c)\,/2N_cN_bE}{\int_{t_1}^{t_2}\sigma_{Au}(t')\frac{\tilde{C}(t')}{t'}(1 - \gamma - e^{-\Sigma_{Cd}(t')s})\,dt'}, \tag{17}$$

from the counting rates $\tilde{C}(t)$ taken during the activation experiment, or from Equation 8, if using a value of K generated in a previous experiment. The cadmium-difference technique thus permits the spectrum normalization to take place even without monitor data at higher neutron energies, corresponding to time-of-flight less than t_1, where recovery from the initial prompt radiation pulse distorts the response of the detector, and where resonance effects complicate the interpretation of activation data.

The rates at which the foils are activated, R_b and R_c, are obviously equal to the saturation activity of those same foils. The saturation activity a_∞ can be determined from

$$a_\infty = \frac{a_x}{1 - e^{-\lambda_{Au}t_x}}, \tag{18}$$

where t_x is the time of exposure, λ_{Au} is the decay rate of the activation product, and a_x is the foil activity at the end of a short exposure.

2.2 Pulse Shapes

The time-dependence of the neutron emission from the moderator surface is a strong determinant of the resolution which can be achieved in any experiment involving the neutron beam. These pulse shapes have been measured, as a function of neutron energy, using a time-focused crystal analyzer system.[3,4] Figure 3 shows such a time-focused crystal analyzer.

The quantity measured in such an experiment is simply a counting rate as a function of time. A crystal reflects a series of mono-energetic pulses to a detector. The operation of the time-focused crystal analyzer is such that the dominant instrumental contribution to the resolution of the measurement is the flight time of the neutrons across a 1 mm thick crystal and their lifetime in a 1 mm thick detector. Thus, the peak shape of the counts registered in the detector matches the time distribution of the neutrons leaving the moderator surface, delayed by the known flight time of each order of reflection.

In the Monte Carlo calculations, this quantity is determined by tallying the neutrons leaving the viewed surface of the moderator as a function of time from the initial source pulse. The difference between the simulation and measurement is then limited to the minimal instrumental resolution and the flight time of the neutrons from the moderator to the detector. Unfortunately, this tally does not benefit from the use of the point detector method described below, although it does benefit from the weight windows.

Experimentally, this time distribution can be measured on a pulsed source by using a crystal analyzer to select a discrete set of neutron energies that are reflected to a detector. As in any crystal spectrometer, the mosaicity of the analyzer combines with the width and angular divergence of the beam to define the portion of phase space containing neutrons that will reach the detector. This can be represented as

$$R \sim \Delta\theta_{\mathrm{B}} \cot\theta_{\mathrm{B}}. \tag{19}$$

The challenge in making such a measurement comes about because the resolution required to accurately measure short neutron pulses (such as we see with at IPNS) implies small, tightly collimated beams, and thus low counting rates. Equation 19 indicates that the resolution can be improved (i.e., reduced) by using the spectrometer in a backscattering config-uration—as the Bragg angle θ_{B} approaches 90°, the resolution R becomes small. Unfortunately, such backscattering geometries can be somewhat difficult to use, especially when working around other dedicated instruments and associated equipment.

The backscattering analyzer can be generalized to function at other scattering angles if the correlations between scattering angle, scattering vector, and flight path lengths are accounted for and properly adjusted. Such a generalization becomes the time-focused crystal analyzer as shown in Figure 3. For a beam of transverse extent W and angular divergence α, and a crystal of mosaicity β, the variance of the resolution of such an instrument is (to first order)

$$\sigma^2 = A\alpha^2 + B\beta^2 + CW^2 + \sigma_{\mathrm{c}}^2 + \sigma_{\mathrm{d}}^2, \tag{20}$$

where A, B, and C are coefficients determined by the system geometry:

$$A = \frac{1}{v^2}\left(\frac{L_1 + L_2}{\tan\theta_{\mathrm{B}}} - L_1\tan\theta_{\mathrm{M}} - L_2\tan\theta_{\mathrm{d}}\right)^2, \tag{21}$$

$$B = \frac{1}{v^2\tan^2\theta_{\mathrm{B}}}\left(L_1 + L_2 - 2L_2\tan\theta_{\mathrm{B}}\tan\theta_{\mathrm{d}}\right)^2, \tag{22}$$

$$C = \frac{1}{3v^2}\left(\tan\theta_{\mathrm{M}} - \tan\theta_{\mathrm{c}} + \frac{\sin(2\theta_{\mathrm{B}} + \theta_{\mathrm{c}} + \theta_{\mathrm{d}})}{\cos\theta_{\mathrm{c}}\cos\theta_{\mathrm{d}}}\right)^2. \tag{23}$$

If these coefficients are set to zero, then α, β, and W can be fairly large (increasing the counting rate) without significantly impacting the instrumental resolution. Setting these terms to zero results in the following focused conditions:

$$\tan\theta_{\mathrm{M}} = \frac{1}{2}\left(1 + L_2/L_1\right)\cot\theta_{\mathrm{B}}, \tag{24}$$

$$\tan\theta_{\mathrm{d}} = \frac{1}{2}\left(1 + L_1/L_2\right)\cot\theta_{\mathrm{B}}, \tag{25}$$

$$\cot\theta_{\mathrm{c}} = \frac{\cos\theta_{\mathrm{d}}\tan\theta_{\mathrm{M}} + \sin(2\theta_{\mathrm{B}} + \theta_{\mathrm{d}})}{2\sin\theta_{\mathrm{B}}\sin(\theta_{\mathrm{B}} + \theta_{\mathrm{d}})}. \tag{26}$$

3 Simulation Methods

The simulations reported here were performed using the MCNP (version 4B)[5] and LAHET (version 2.70)[6] computer programs. These codes are extremely popular, and in general quite well validated.[7] Thus, our task is not so much benchmarking the codes as it is benchmarking our application thereof. This includes cross section data specific to cold moderator materials, the geometric model of our system, and the appropriateness and interpretation of our calculated results. These calculations were performed on an eight processor cluster of Pentium-II machines (running Linux), using MCNP's inherent support of the PVM software from Oak Ridge National Laboratory.[8]

MCNP, like any modern Monte Carlo code, has a rich selection of variance reduction features from which to chose. We employed the so-called *Weight Window* and *Point Detector* methods, described below, to speed the convergence of our calculations. Using variance reduction is absolutely essential for obtaining worthwhile estimators of cold neutron production in reasonable amounts of computer time. As an example, consider the calculation of the intensity of neutrons in a typical range of interest, say 4–14 Å. The use of these variance reduction methods speeds the calculation to a specified precision by a factor of 10^4. The MCNP4B manual describes these variance reduction methods in detail.[5] A short description of these methods appears below.

3.1 Weight Windows

Weight window variance reduction is a method of simultaneous space- and energy-dependent splitting and roulette techniques. The basic concept is that, as particles move from one region of phase space to another, more "interesting" region, they are split—i.e., replaced by multiple identical particles with the same total weight as the initial particle. These particles are then followed individually. Conversely, in the roulette instance, particles moving from one region of phase space to a *less* interesting region have some finite probability of being terminated. If the the particle survives the roulette process (the fractional probability of which is p) then its weight is multiplied by $1/p$. This process vastly increases the fraction of CPU time spent on particles in neutronically important portions of phase space, yet does not introduce a bias into the resulting calculations. The use of weight windows requires then some assessment of the importance of each region of phase space sampled within the problem. This importance function can be estimated by a skilled user, or from an adjoint multi-group calculation. MCNP also includes a very effective method for the iterative generation of the importance function.

The phase space importance function used for these calculations was constructed using this automatic generation method (called the Weight Window Generator). The importances thus calculated are subject to statistical errors, as are all quantities calculated by Monte Carlo techniques. In order to speed the convergence of the weight window generator, intermediate results were averaged for "similar" regions of geometrical space. In other words, the weight window generator might, for example, estimate the neutronic importance of several different cells, each of which was physically part of the cadmium decoupler surrounding a given moderator. When these importances are averaged, the statistical variation is smoothed somewhat, and the iterative process converges more quickly.

Finally, the resulting importance function was smoothed, in order to guarantee no severe gradients in the importance function. During the iterative process, the repeated appearance of such severe gradients in a given location indicates that adjacent regions of phase space are "too large." Breaking these regions into smaller ones, either in physical space or in energy space, results in a better importance function and a more efficient calculation.

Using a well-defined importance function can result in interesting regions of phase space (such as a viewed moderator surface between 1 meV and 1 eV) being sampled hundreds of times more frequently than they would be in a strictly analog simulation, with corresponding increases in overall computing speed.

3.2 Point Detectors

The point detector method of variance reduction is not actually a biasing of the random walks in the Monte Carlo calculation, but is instead a next event estimator. One of the great disadvantages of Monte Carlo methods is that they are intrinsically unsuited to calculating a particle flux at a given point, as opposed to averaging over a large volume. Since the production of neutron beams is essentially a low probability streaming problem, a strictly analog Monte Carlo calculation would almost never track particles in the small portion of phase space that is of interest.

If one is interested in the flux at a given location, one can instead deterministically calculate the probability that a particle at any other given point in space will contribute to the flux at that location. In MCNP, this is implemented as the point detector. At every scattering event, the transmission probability from the scattering event location to the detector location is calculated, and the point detector tally is augmented by the product of that probability and the particle's weight. Thus every single collision which takes place anywhere in the system contributes to the calculation, as opposed to only the miniscule fraction of the particles that happens to leak through the system in the correct direction.

Consider a perfectly moderating material—i.e., all scattering is inelastic, and there is no absorption. A source neutron entering this moderator has perhaps 5 MeV of energy, and will eventually leak out of the moderator. If one considers only the viewed face of the moderator, the chance that the neutron leaks out of the appropriate face is approximately 25%. Thus a tally recording all leakage through the viewed moderator face records some 0.25 contributions per source particle.

In an hydrogenous material, a 5 MeV neutron requires about twenty inelastic collisions to reach energies of 1 meV. Using a point detector, every one of those collisions contributes to the detector. Even when one considers only those scattering events below, say, 10 eV, there are a minimum of eight to ten collisions that result in desirable contributions to the tally. Once elastic collisions are included, each source particle can contribute to the tally up to twenty times or more. Thus the efficiency of the calculation per source particle increases by nearly two orders of magnitude. This increase comes at a relatively trivial cost of some ten percent or less in CPU time per source particle. This hundred-fold increase in calculation speed, when multiplied by the similar increase described above from the weight window methods, can turn a calculation that might take the better part of a year into one which will be completed in an hour with the same statistical precision.

3.3 Scattering Kernel Data

The accuracy of any Monte Carlo simulation is limited by the accuracy of the scattering kernel data used in the simulation. This is especially true in the case of under-moderated, time-dependent systems such as those we are studying. The scattering kernels of greatest importance are those for the cryogenic moderator materials. The kernels that are widely available for use with MCNP appear in Table 1, and are a part of the standard MCNP distribution. These kernels are described in greater detail elsewhere.[9] The kernels we have

Material	(K)	Material	(K)
Solid Methane	22	Liquid Methane	100
Para Hydrogen	20	Para Deuterium	20
Ortho Hydrogen	20	Ortho Deuterium	20

Table 1: Cryogenic moderator material scattering kernels available for use with MCNP.

used in these calculations are test versions of these same kernels, evaluated to somewhat higher accuracy, and at additional temperatures. These kernels are also further described elsewhere,[10] and will hopefully be

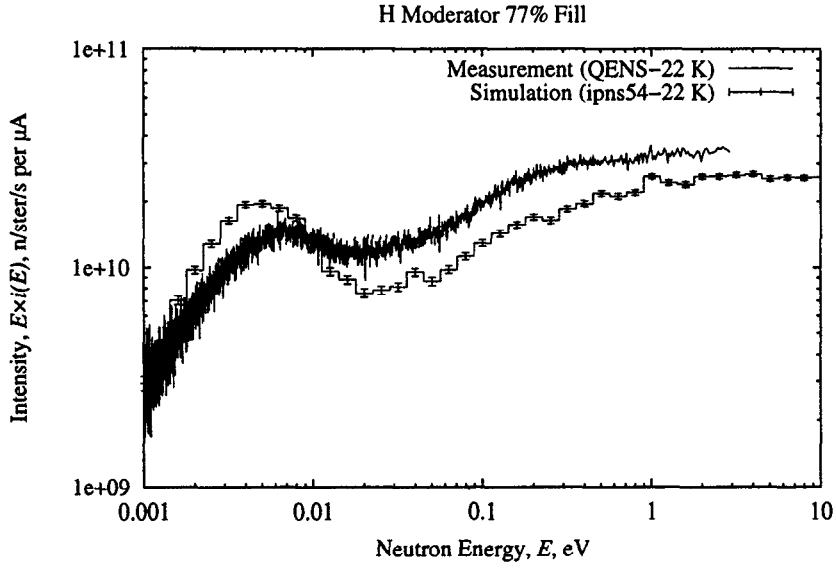

Figure 4: Absolute spectral intensity as measured on QENS from the 22 K solid methane "H" moderator.

available for general use at the time of this publication.

4 Results

We have compared the output of our Monte Carlo simulations to corresponding measurements made on the IPNS system. We have examined results from all three of the existing moderators, and we have examined both spectral intensities and wavelength/energy dependent pulse shapes. We have examined moderators composed of both liquid and solid methane, moderators with and without heterogeneous poisoning, and moderators of reentrant and non-reentrant geometries.

4.1 Spectral Intensities

We have measured the absolute spectral intensities of the neutron beams on several IPNS beam-lines. Here we will only discuss the measurements on two of these beam-lines—the QENS beam-line, viewing the solid methane "H" moderator, and the SEPD beam-line, viewing one side of the liquid methane "F" moderator. A more complete description of these measurements appears elsewhere.[11]

In the case of the solid methane moderator, the scattering kernel information used in the simulations corresponds to a temperature of 22 K, rather than the 30 K at which our solid methane moderators normally operate. With this in mind, we operated the solid methane "H" moderator at 22 K for a short time during a dedicated machine research period. The absolute spectral intensity for the QENS beam line (normal to the moderator surface), as measured at 22 K using the efficiency determined with a gold foil activation run at 30 K, is shown in Figure 4, together with the corresponding simulation results. This simulation tracked approximately 10^8 neutrons, of which some forty percent were original (spallation) source neutrons, as produced by the LAHET code following 5×10^4 450 MeV proton cascades. The point detector tally used recorded contributions not only from collisions within the moderator volume, but also from the portions of the graphite reflector which are nominally viewed through the beam line collimation, albeit perhaps after transmission through moderator and decoupler regions.

The intensity was measured over a period of approximately one hour, at an average proton current of

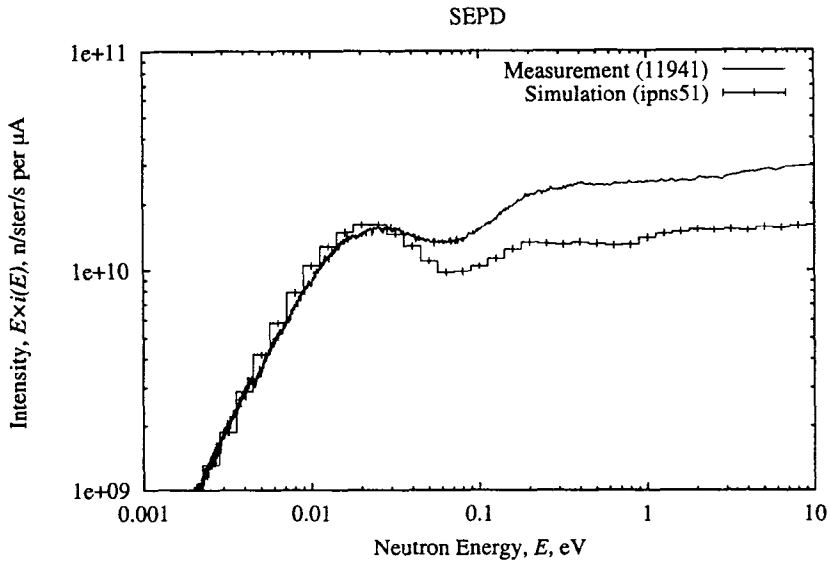

Figure 5: Absolute spectral intensity as measured on SEPD from the 100 K liquid methane "F" moderator.

12.36 μA. The measured moderator coupling is 3.3×10^{10} neutrons per steradian per second per micro-Ampere of proton current. This quantity represents the integral over the entire 100 mm by 100 mm viewed surface of the moderator. The simulation predicts a moderator coupling some 30% less than actually observed. Furthermore, the shapes of measured and simulated spectra do not match very well at all, as discussed further below. The nominal (measured) time-averaged moderator brightness at 1 eV, assuming constant proton operation at 14 μA, is 4.6×10^{13} neutrons per steradian per second per square meter.

The liquid methane "F" moderator is typically operated at 100 K, matching the temperature in the scattering kernel library. We measured the spectral intensity for the liquid methane moderator on the SEPD beam-line, normal to one side of the "F" moderator. Figure 5 shows the absolute spectral intensity as measured, again with the corresponding simulation results. These Monte Carlo results came from the same simulation as described above, tracking approximately 10^8 neutrons, as produced by the LAHET code following 5×10^4 450 MeV proton cascades and subsequent multiplication by both variance reduction methods and physical processes. This point detector tally also recorded contributions from viewed portions of the reflector as well as from the moderator volume, although the "F" moderator is distinct in that there is no reflector region immediately "behind" the moderator, as the moderator is viewed from both sides.

The intensity was measured over a period of some ninety minutes, at an average proton current of 13.95 μA. The measured moderator coupling is 2.4×10^{10} neutrons per steradian per second per micro-Ampere of proton current. As before, this quantity represents the integral over the entire 100 mm by 100 mm viewed surface of the moderator. The simulated moderator coupling and subsequent average brightness is lower than that measured by approximately 30% (1.7×10^{10} and 2.3×10^{13}, respectively). The nominal moderator brightness at 1 eV, assuming constant proton operation at 14 μA, is 3.3×10^{13} neutrons per steradian per second per square meter.

4.2 Pulse Shapes

The pulse shapes of the flat liquid methane "F" moderator, the grooved solid methane "C" moderator, and the flat solid methane "H" moderator have been measured. These measurements were performed, as de-

n	λ (Å)	E (meV)	v (km/s)
1	5.686	2.531	0.6958
3	1.895	22.78	2.087
4	1.421	40.49	2.783
5	1.137	63.27	3.479
7	0.8123	124.0	4.871
8	0.7107	162.0	5.567
9	0.6318	205.0	6.262
11	0.5169	306.2	7.654
12	0.4738	364.4	8.350
13	0.4374	427.7	9.046
15	0.3791	569.4	10.44
16	0.3554	647.8	11.13
17	0.3345	731.3	11.83
19	0.2993	913.6	13.22
20	0.2843	1012	13.92
21	0.2708	1116	14.61

Table 2: The allowed (nnn) reflections from germanium at 25 K and $2\theta = 120°$.

scribed above, using a time-focused crystal analyzer based on the (nnn) series of reflections from a cooled germanium crystal. The pulse shapes were only measured for neutron energies corresponding to these reflections at the specific scattering angle, in this case $2\theta = 120°$. Table 2 lists these reflections.

The fourth order reflection (40.49 meV neutron energy) as measured on the liquid methane "F" moderator appears in Figure 6, together with the corresponding simulation results. Space limitations prohibit the inclusion of all of the pulse shapes measured. However, one significant metric describing the neutron pulses is the pulse width. The measured pulse width as a function of neutron wavelength appears in Figure 7, and is compared to the simulated value. Note that Figure 7 does not show the often quoted full-width at half-maximum of the pulse, but rather the time width of the central eighty percent of the integrated pulse area. This metric is somewhat more robust than the FWHM for noisy pulses—the counting statistics on the measured pulses are rather poor at both extremes of the measured range, and the Monte Carlo precision is rather poor at the long-wavelength end of the range. This metric is also more sensitive to the tails of the pulses, which are poorly sampled in the simulation.

The 40.49 meV pulse shape for the solid methane "C" moderator appears in Figure 8, from both measurement and simulation. The measured pulse width for the "C" moderator as a function of neutron wavelength appears in Figure 9, and is compared to the simulated value. Finally, the pulse width from the flat, poisoned solid methane "H" moderator appears in Figure 10.

5 Discussion

The results of our simulations do, to a large extent, show strong similarity to the corresponding measurements. There are, as discussed below, some difficulties with the neutron moderation predicted in solid methane, but these difficulties are not so pervasive that we cannot use the simulation model for the optimization and analysis studies which we wish to perform. That is, we think that the calculated changes will be reliable enough to support many optimization decisions.

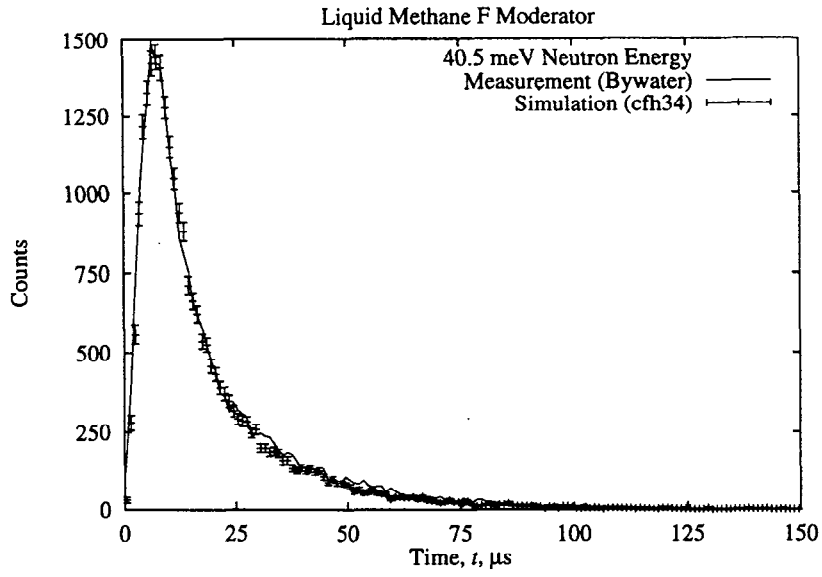

Figure 6: Time-dependent pulse shape for Ge (444) neutrons from the 100 K liquid methane "F" moderator. The line represents the measured data, while the points are the simulation results.

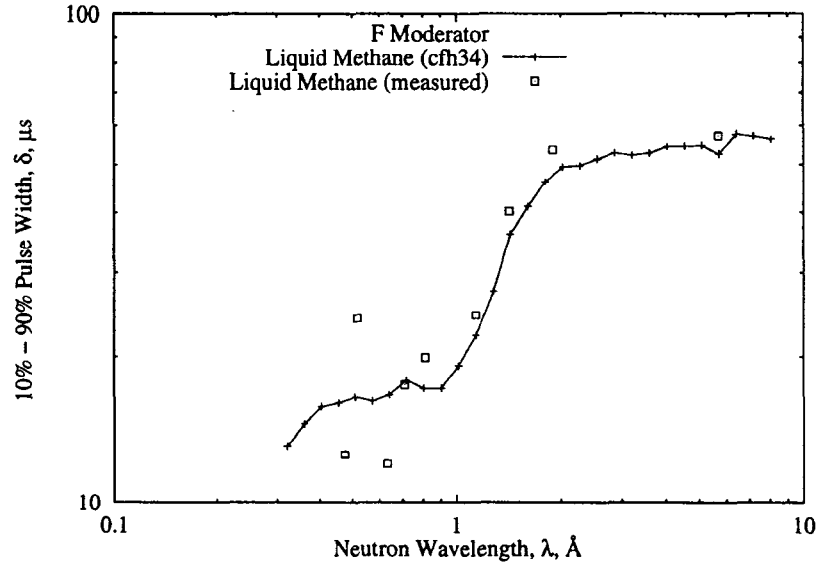

Figure 7: Pulse width as a function of neutron wavelength for the liquid methane "F" moderator.

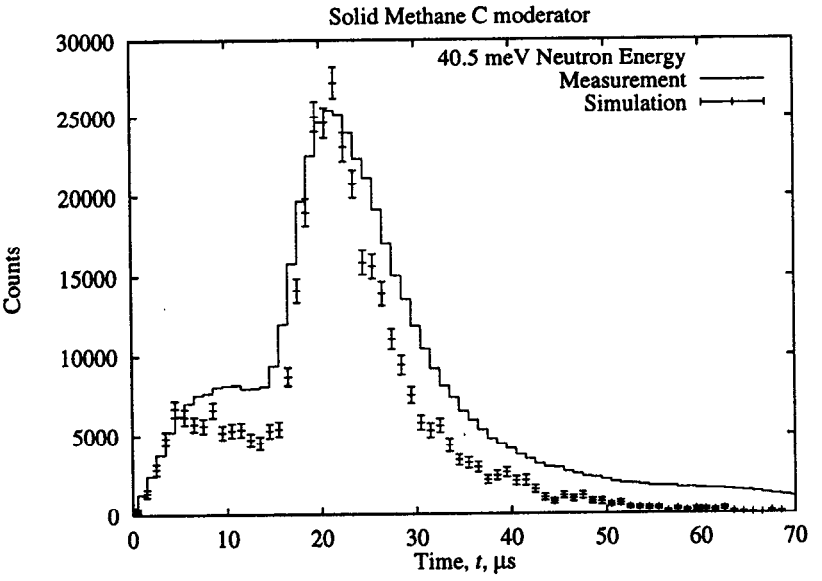

Figure 8: Time-dependent pulse shape for Ge (444) neutrons from the 30 K grooved solid methane "C" moderator.

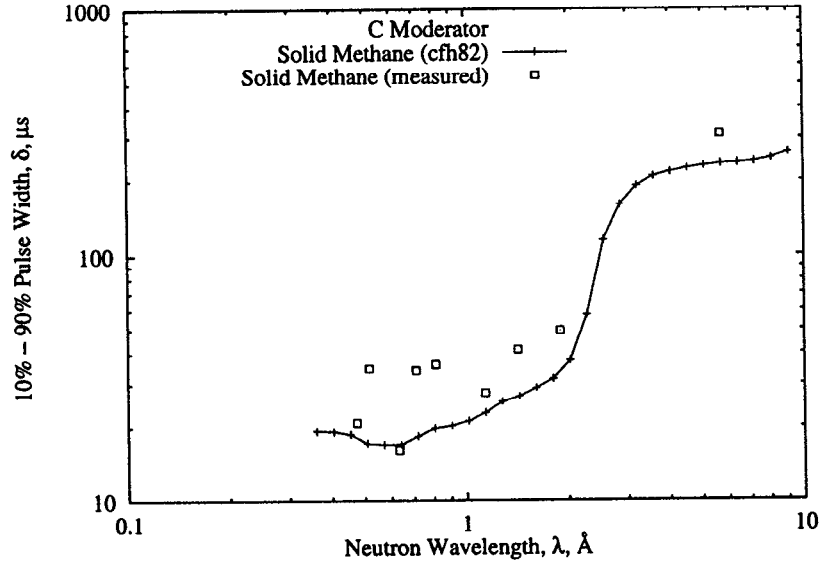

Figure 9: Pulse width as a function of neutron wavelength for the grooved solid methane "C" moderator.

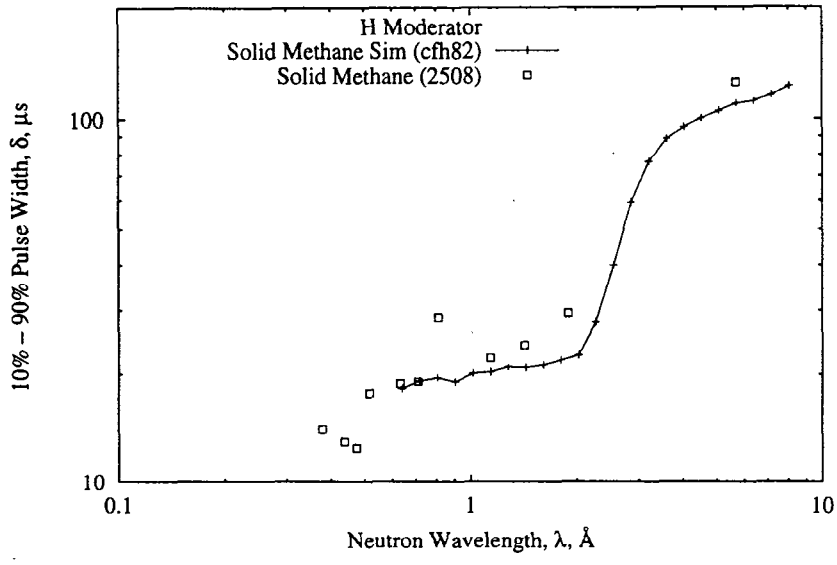

Figure 10: Pulse width as a function of neutron wavelength for the flat, poisoned solid methane "H" moderator.

5.1 Spectral Intensities

Figure 4 compares the results of simulation and measurement for the spectral intensity of the solid methane "H" moderator. While the spectrum displays many qualitative similarities, there are obvious, considerable discrepancies. The moderator coupling (the intensity at 1 eV) is under-predicted by some 30%. This is in contrast to earlier results,[1] which indicated good agreement for this parameter. The only significant aspect of the simulation which has changed in that time is a more accurate treatment of the high energy source term. Therefore, we believe that the inaccuracy in the coupling is due to flaws in the model-based calculation of neutron source term from the proton spallation on the uranium target. Similar errors have been reported elsewhere for spallation neutron production from uranium at a proton energy around 500 MeV.[12]

Furthermore, in the thermalized portion of the spectrum, there are great differences in the spectral shape. These discrepancies are so pervasive that the spectral temperature of the moderator is incorrectly estimated, as well as the actual thermal flux, as might be characterized by the thermal-to-epithermal ratio. The measured spectral temperature is approximately 4.2 meV (49 K), while the simulated spectral temperature is about 2.5 meV (29 K). Note that the maximum value of a Maxwellian in $i(E)$ when expressed as $E \times i(E)$ is located at $2k_BT$. Furthermore, the cutoff energy, defined as that energy where the flux changes from a $1/E$ behavior to a Maxwellian behavior, occurs at a significantly different energy in the simulation from that actually observed. As a result, the simulation significantly under-predicts moderator performance from 10 meV to 1 eV, the range most relevant to, say, powder diffraction and chopper spectrometer measurements, and significantly overpredicts moderator performance for cold neutrons, as relevant to quasi-elastic scattering and small-angle diffraction.

Finally, the simulated spectrum has some non-physical features, including discontinuities, below 1 eV. It is worth noting that the simulation treats the molecular scattering kernels in detail at neutron energies of 950 meV and below. The increased onset of inaccuracies and non-physical features just below 1 eV seems indicative of some problems with the scattering kernel data, coming from either inaccuracy in the molecular

description, or from discretization error in that description. The kernel is stored, in the code, as a set of equally likely final energies for each initial energy, and a set of equally likely scattering angles for each pair of energies. For this solid methane kernel, there are sixteen final energies for each incident energy, and sixty-four scattering angles for each pair of energies. The non-physical features observed are much less than those previously observed in kernels with eight energies and sixteen angles.[1]

The accuracy of the simulation of the liquid methane spectrum, as in Figure 5, is somewhat better. While the coupling and the thermal-to-epithermal ratio have discrepancies on the order of 30–50%, they offset such that the thermal flux predicted by the simulation is nearly identical to that measured. The spectral temperature is predicted very accurately. Another difficulty with the liquid methane simulation is, again, the non-physical features caused by discretization errors in the scattering kernel representation.

We previously reported[1] that the two spectra, when taken together, might indicate a possible problem in the geometric model of the system, given that the moderator coupling was accurately predicted in the case of the solid methane moderator, but not in the case of the liquid methane moderator. This no longer appears to be the case; the coupling is under-predicted by some 30–50% in each case. We feel that this is further evidence that the likely origin of the problem is the physics model for spallation in uranium at 500 MeV proton energy.

5.2 Pulse Shapes

The simulated pulse shapes from the liquid methane "F" moderator match the measured pulse shapes very well, as seen in Figure 6. Similarly, the pulse widths as shown in Figure 7 seem to behave very similarly.

The solid methane simulations were not so successful. There are significant differences in the relative heights of the the bimodal peak from the grooved moderator, as seen in Figure 8. The under-prediction of the height of the earlier peak (from the tips of the moderator fins) also results in an under-prediction of total pulse width. Examination of Figure 9 clearly shows that the solid methane simulation consistently under-predicts observed pulse widths by 30% to 40% over all wavelengths. On a more positive note, the rise time of the pulse appears to be accurately predicted. This is quite important for many instruments, as the resolving power of the instrument is largely determined by the sharpness of that rise time, as opposed to the total width of the pulse. The under-prediction of pulse widths is also seen for the flat solid methane "H" moderator in Figure 10, although not as severely as for the grooved moderator.

It is further obvious that the selection of neutron wavelengths at which the pulse shape was measured is not well matched to the physics of the solid methane system. The sharp increase in pulse width, corresponding to the increasing importance of the storage term in the pulse shape as the neutrons come into thermal equilibrium with the moderator material, is very inconveniently located in the exact range that is not measured at all in the germanium (nnn) series of reflections through $2\theta = 120°$. These measurements should be repeated for a set of wavelengths that will better match the characteristics of the solid methane moderators.

6 Conclusions

The Monte Carlo simulation of the methane moderators at IPNS shows clear difficulties with the solid methane scattering kernel as implemented with the MCNP computer code. These problems take the form of significant errors in the spectral temperature, intensity, and pulse shapes of the moderated neutron flux. These errors are not as severe in the liquid methane simulations. Furthermore, the simulations show a consistent under-prediction of the neutron production rate from the target, matching previous observations from the literature.

While these discrepancies are significant enough to warrant serious attention, we do believe that the comparison between the measurements and the simulations is good enough that we can consider our simulation model useful for some aspects of the target, moderator, and reflector system—e.g., target design, reflector material, moderator position. For studies involving detailed study of neutron moderation in solid methane,

however, our model requires further development and testing. The model will be more valuable for observing trends and making optimizations, certainly, than it will for making absolute predictions.

One avenue for further testing involves comparison of the scattering kernel used in the simulations to a scattering kernel actually measured on an inelastic neutron spectrometer. We propose that such measurements be undertaken over a wide range of Q- and ω-space for solid methane at the temperature used in the development of the simulation data. Such a program of measurements could further be extended to cover novel moderator materials, as well as conventional moderator materials at a wider range of temperature and pressure conditions than has been considered previously.

Finally, some of the measurements used for these comparisons should be extended. While the intensity measurements appear to be satisfactory, the pulse shape measurements, using this particular crystal analyzer arrangement, do not have sufficiently dense wavelength coverage. The germanium (nnn) series used reflects an adequate selection of wavelengths for the liquid methane moderators, but not for the solid methane moderators, as no reflections exist in the critical region between two and five angstroms where the pulse width changes most rapidly.

References

[1] E. B. Iverson and J. M. Carpenter. Benchmarking simulation methods for methane moderators. In John M. Carpenter and Erik B. Iverson, editors, *Proceedings of the International Workshop on Cold Moderators for Pulsed Neutron Sources*. OECD, 1998.

[2] E. B. Iverson, J. M. Carpenter, and E. J. Hill. Cold neutron beams at the Intense Pulsed Neutron Source. *Physica B*, 241–243:33–35, 1998.

[3] K. F Graham and J. M. Carpenter. Pulsed moderator studies using a time focussed crystal spectrometer. *Nuclear Instruments and Methods*, 85:163–171, 1970.

[4] Russel Lee Bywater, Jr. Neutron emission-time distributions of methane moderators at the Argonne National Laboratory Intense Pulsed Neutron Source. Master's thesis, Iowa State University, August 1989.

[5] Editor Judith F. Briesmeister. *MCNP—A General Monte Carlo N-Particle Transport Code*. Los Alamos National Laboratory, March 1997. Version 4B.

[6] Richard E. Prael and Henry Lichtenstein. *User Guide to LCS: the LAHET Code System*. Los Alamos National Laboratory, September 1989.

[7] John S. Hendricks and John D. Court. MCNP4B^{TM} verification and validation. Technical Report LA-13181, Los Alamos National Laboratory, August 1996.

[8] Al Geist, Adam Beguelin, Jack Dongarra, Weicheng Jiang, Robert Mancheck, and Vaidy Sunderam. PVM 3 User's Guide and Reference Manual. Technical Report ORNL/TM-12187, Oak Ridge National Laboratory, September 1994.

[9] R. E. MacFarlane. New thermal neutron scattring files for ENDF/B-VI release 2. Technical Report LA-12639-MS, Los Alamos National Laboratory, August 1994.

[10] G. J. Russell and R. E. MacFarlane. Report of the Working Group on scattering kernels and cross sections. In John M. Carpenter and Erik B. Iverson, editors, *Proceedings of the International Workshop on Cold Moderators for Pulsed Neutron Sources*. OECD, 1998.

[11] E. B. Iverson, J. M. Carpenter, and E. J. Hill. Absolute beam intensity measurements at the Intense Pulsed Neutron Source. In John M. Carpenter and Erik B. Iverson, editors, *Proceedings of the International Workshop on Cold Moderators for Pulsed Neutron Sources*. OECD, 1998.

[12] Bruce W. Patton, Gary J. Russell, James S. Gilmore, Phillip D. Ferguson, John D. Court, and Eric J. Pitcher. Benchmarking of the fertile to fissile conversion FERFICON water bath experiments: Integral n/p measurements. In *Topical Meeting on Nuclear Applications of Accelerator Technology*, pages 229–234. American Nuclear Society, November 1997.